Mathematical Biosciences and Engineering

MBE, 18(5): 6907–6925.
DOI: 10.3934/mbe.2021343
Received: 18 June 2021
Accepted: 15 August 2021
Published: 20 August 2021

http://www.aimspress.com/journal/MBE

Research article

Characterisation of transient electromagnetic signals during fixed interference sources in tunnel structure

Wangping Qian[1,2], Yikang Xu[1], Zhenyuan Gu[1], Ziru Xiang[1,*], Zongyang Li[2], Jinchao Liu[2] and Jiujiang Wu[1]

[1] School of Transportation and Civil Engineering, Nantong University, Nantong 226019, China

[2] Key Laboratory of Transportation Tunnel Engineering Ministry of Education, Southwest Jiaotong University, Chengdu 610031, China

* **Correspondence:** Email: ziruxiang@ntu.edu.cn.

Abstract: The detection effect of the transient electromagnetic method is ambiguous in engineering applications due to the existence of interference sources, so explaining the influence of these fixed interference sources on is crucial. In this paper, the response characterisation of transient electromagnetic signals of fixed interference sources are thoroughly investigated. First, the secondary field generated by these interference sources is analyzed, and a typical fixed interference source is calculated. Then, a sensitivity analysis of the transient electromagnetic response curve is carried out. Finally, the mathematical superposition method for multiple field sources is proposed and verified. The results illustrate that the transient electromagnetic response curve of uniform full-space surrounding rock with a single fixed interference source has an apparent lifting phenomenon in the middle stage and presents an approximate horizontal change rule at the late stage. The transient electromagnetic response curves of multiple field sources separately illustrate the response characterisation of different field sources at different time stages. These research results can provide a valuable reference for the on-site interpretation of detection signals.

Keywords: transient electromagnetic signal; interference source; response characterisation; sensitivity analysis; mathematical superposition

1. Introduction

In recent years, many tunnels have been put into operation with the rapid construction of high-speed railways in China [1]. However, the operation situations of tunnels are not optimistic according to field investigations, and there are many tunnel defects, especially internal defects such as water leakage and cavities [2,3]. The rapid detection of these internal defects is of great significance to the maintenance of high-speed railway tunnels. In view of the detection characterisation of the transient electromagnetic method (TEM), this method has been gradually proposed and applied to the rapid detection of operational tunnel defects [4–6]. However, similar to TEM, this method has an interpretation problem of interference sources in the measured signal data.

In the application engineering field of TEM, an interference source at the detection site is inevitable, and the existence of an interference source has an important influence on the interpretation of transient electromagnetic detection data [4]. For this reason, many geophysicists have studied the interference source at the detection site. Liu et al. [7] investigated the influence of excavation trolleys and steel arches in tunnel space via field detection tests and laboratory physical experiments. A recommended distance of metal interference away from the excavation face and transmitter coil was also given. Sun et al. [8] demonstrated the response law of advanced tunnel detection under the condition of an interference source of a tunnel boring machine through numerical simulations and theoretical research methods. The interference source of a tunnel boring machine illustrates the electromagnetic characterisation of low-resistivity targets and can be removed by theoretical superposition. Zhou et al. [9] performed a detailed analysis on induced polarization distorted TEM data based on numerical simulation and field examples, and the induced polarization effect of single-line and double-line grounded-wire sources was compared. Wu et al. [10] adopted a deep learning method to remove a specific type of interference noise, including motion-induced noise, nearby or moderately distant sferics noise, power-line noise and background electromagnetic noise. The research illustrated that the respective characterisation of the signal and interference noise can be identified and distinguished. Blanco-Arrué et al. [11] developed a transient electromagnetic study in the noisy urban environment of the megacity Santiago de Chile and identified different transient characterisation and noise patterns spatially correlated to the investigation area. Tamburrino et al. [12] extracted the distance parameter between the probe and defect of a canonical inverse problem in a full three-dimensional time-domain problem of defect detection. Sophina et al. [13] systematically introduced time-domain features and frequency-domain features in the field of pulsed eddy current nondestructive testing and evaluation, and dimensionality reduction techniques used in feature extraction for pulsed eddy current signals were introduced. Li et al. [14] proposed four time-domain features of transient electromagnetic signals in advanced geological prediction of a tunnel and successfully predicted defects in front of the tunnel face. Qian et al. [4] proposed five time-domain features of transient electromagnetic signals in tunnel defect detection. Based on an investigation of interference sources or defects, these studies greatly enriched the theoretical research of interference sources on TEM and improved the inversion accuracy of TEM by reducing the interpretation influence of field data.

Many interference sources can be avoided in the process of transient electromagnetic detection by moving away during underground water and metal mineral exploration in coal mines, tunnels and the ground [6,8,14–16]. Moreover, the influence of interference sources on the detection signal can be minimized. Unfortunately, tunnel interference sources always exist and cannot be averted in the process of operating tunnel disease detection. The transient electromagnetic signal induced by multiple

field sources is a symbiosis during the process of vehicle-mounted transient electromagnetic detection, which means that the ineffective and effective electromagnetic signals of multiple field sources appear, weaken and disappear simultaneously [4,17]. Therefore, the performance characterisation of the transient electromagnetic signals of a fixed interference source in all signals are worthy of further investigation, and the correlation between these signals needs to be deeply studied.

This paper investigates the detection influence of interference sources on transient electromagnetic response signals in three-dimensional space. A typical fixed interference source is selected as the analysis object, and the transient electromagnetic response characterisation of the fixed interference source are fully researched via theoretical analysis and numerical simulation. The induced current generated by the fixed interference source is analyzed, and a simplified form of a fixed interference source is proposed. The transient electromagnetic response curve of the fixed interference source is calculated, and the different phenomena are illustrated and compared with the calculation results of uniform full-space surrounding rock and water-bearing bodies. In addition, a sensitivity analysis of a fixed interference source is calculated and revealed in different physical parameters, including the distribution length, distribution interval and diameter. Finally, the mixed electromagnetic signals produced by multiple field sources are investigated, and a mathematical superposition method is proposed and verified to obtain an effective detection signal of the surrounding rock. This research can provide theoretical guidance for the identification and separation of interference sources in vehicle-mounted transient electromagnetic detection.

2. Electromagnetic response characterisation of a fixed interference source

2.1. Analysis principle of transient electromagnetic fields

According to the basic principle of the transient electromagnetic method, the secondary electromagnetic field of a homogeneous medium in three-dimensional space can be obtained as Eqs (1)–(3).

$$H_R = \frac{2M}{4\pi R^3}[\varphi(u) - \sqrt{\frac{2}{\pi}} u e^{-(u^2/2)}]\cos\theta \tag{1}$$

$$H_\theta = \frac{2M}{4\pi R^3}[\varphi(u) - \sqrt{\frac{2}{\pi}} u(1+u^2) e^{-(u^2/2)}]\sin\theta \tag{2}$$

$$E_\varphi = \sqrt{\frac{2}{\pi}} \frac{M\rho}{4\pi R^4} u^5 e^{-(u^2/2)} \sin\theta \tag{3}$$

where H_R and H_θ are the secondary magnetic field components in spherical coordinates (A/m); E_φ is the secondary electric field component in spherical coordinates (V/m); R, θ and φ are the three components of the spherical coordinates; M is the magnetic dipole moment of the transmitter coil (A·m^2); $\varphi(u)$ is the Gaussian integral ($\varphi(u) = \sqrt{\frac{2}{\pi}} \int_0^u e^{-(t^2/2)} dt$); u is the judgment coefficient of time

or distance of the electromagnetic field ($u = 2\pi R / \sqrt{2\pi\rho t \times 10^7}$); ρ is the resistivity of the space medium (Ω·m); and t is the electromagnetic field time (s).

According to Eqs (1)–(3), the conductive current is initially concentrated near the field source and tries to maintain the magnetic field generated by the original current flow when the current is instantaneously disconnected ($t = 0$). This phenomenon is consistent with the phenomenon of induced electromotive force generated by the changing magnetic field described by Faraday's law. When the induced current gradually begins to diffuse into the surrounding space, the maximum value of the current density amplitude moves toward a large distance based on Eq (3). Meanwhile, the transient electromagnetic field can be simplified as a function of time and dielectric conductivity. Consequently, the electromagnetic field diffuses outward with the increase of time after the dipole source current is turned off. Thus, the magnetic field or induced electromotive force measured near the field source is gradually more sensitive to the eddy current far from the medium.

In the space of vehicle-mounted transient electromagnetic detection, there are also two types of interference sources in addition to the surrounding rock and tunnel lining internal defects. These are called multiple field sources. The first type is the interference source of the tunnel structure, such as a preliminary support or secondary lining. The second type is the interference source of vehicle-mounted detection systems such as vehicle-mounted equipment. Compared with a water-bearing body [4], these interference sources in the tunnel environment are fixed and generally depend on the design scheme of tunnel engineering and vehicle-mounted detection systems. The transient electromagnetic response generated by these fixed interference sources does not change with the position of the vehicle-mounted detection system.

Similar to Eq (3), the electromagnetic induction signal generated by the fixed interference source mainly depends on the propagation time and the distribution of spatial resistivity when other conditions remain unchanged. Thus, the electromagnetic response of the entire space depends on the equivalent resistivity between the surrounding rock and the interference source. To some extent, the second type of interference source can be avoided, such as in nonmetallic equipment, so the first type of fixed interference source is the focus of this research. In the composition of the space medium, the first type of fixed interference source mainly involves concrete and steel mesh. The resistivity of concrete is basically the same as that of the surrounding rock, while the resistivity of the steel mesh is significantly different from that of the surrounding rock, and there is a large magnitude gap between them. As a result, the first type of fixed interference source can be approximately equated with the steel mesh model. Meanwhile, the layout, form and distance of the steel mesh in the tunnel structure are specific for a given tunnel's engineering. Thus, the electromagnetic induction signal generated by the fixed interference source of the steel mesh is basically unchanged.

Based on the above theoretical analysis, the electromagnetic induction signal of space mainly depends on the distribution of the space medium. Therefore, the electromagnetic response characterisation generated by the fixed interference source can be investigated similarly to the homogeneous medium.

2.2. Model simplification based on numerical simulation

The fixed interference source of the steel mesh mainly depends on the layout and form of the steel mesh inside the tunnel structure [8,16]. Multiple steel meshes in the normal direction are temporary

and not considered in this research, and the normal connection of the steel mesh can be ignored. The structural form of steel mesh is a slender and closed loop, so the fixed interference source of steel mesh in the tunnel structure can be simplified as a metal mesh model. Because the diameter of the metal mesh is generally only 10~30 mm, the mesh is far smaller than the general size of the water-bearing body, and the size difference between the two is more than 100 times. To realize a three-dimensional numerical simulation of the metal mesh model, the number of element grids in the three-dimensional model of the metal mesh will show explosive growth compared with the ordinary transient electromagnetic three-dimensional model. In the process of finite element calculation, an increase in the number of element grids readily leads to the nonconvergence of Maxwell's equation, and the calculation time increases exponentially. On the basis of limited computer performance, it is necessary to simplify the simulation of steel mesh to investigate the transient electromagnetic response characterisation of the fixed interference source.

According to the Biot-Savart law, the magnetic field generated by any current element in three-dimensional space can be known as Eq (4). In the Biot-Savart law, the diameter of the steel bar is ignored, and the magnetic field in space generated by the total current depends mainly on the length of the steel bar.

$$dB = \frac{\mu_0}{4\pi} \frac{Idl \sin\theta}{r^2} \tag{4}$$

where dB is the magnetic field generated by the current element (Wb/m^2); I is the current of the current element (A); dl is the length of the current element (m); θ is the angle from any point outside the current element to any point on the current element (rad); and r is the normal distance from any point outside the current element to the current element (m).

From Eq (4), the magnetic induction intensity of any current conductor at any point in space can be obtained as Eq (5).

$$B = \int_L dB = \int_L \frac{\mu_0}{4\pi} \frac{Idl \sin\theta}{r^2} \tag{5}$$

where B is the magnetic induction intensity of any current conductor at any point in space (Wb/m^2) and L is the integration path.

For the rectangular loop frame, it is assumed that the length of the loop frame is L, and the magnetic field generated at the center point is $B = \frac{2\sqrt{2}\mu_0 I}{\pi L}$ according to Eq (5). For a circular loop, assuming that the diameter of the loop frame is also L, the magnetic field generated at the center point is $B = \frac{\mu_0 I}{L}$. Comparing the magnetic field generated by the rectangular and circular loop frames at the center point, it can be illustrated that the two forms are the same, and there is only a certain multiple relationship, so these two forms can be equivalent.

On the basis of rectangular wireframes, a rectangular steel mesh with five intervals is selected as the analysis object, and the uniform and nonuniform distribution magnetic fields generated in the space of the steel mesh are shown in Figure 1. In Figure 1, B_0, B_1 and B_2 represent magnetic fields in different regions. It is assumed that the center of the cupper transmitter coil is on the same axis as the center of the steel mesh. The magnitude and direction of magnetic fields in different regions depend on the magnitude and direction of the current in the upper transmitter coil. The direction of the current

in the upper transmitter coil is counterclockwise, so the direction of the electromagnetic field is from the inside to the outside in Figure 1.

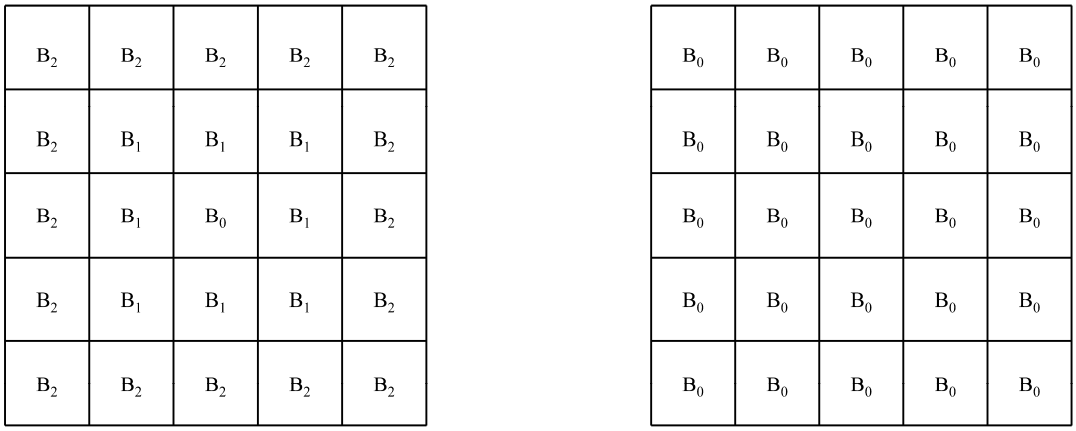

(a) Nonuniformly distributed magnetic field (b) Uniformly distributed magnetic field

Figure 1. Distribution of magnetic fields in space under two conditions.

When the primary field changes in three-dimensional space, an induced current is produced in the steel mesh. Assuming that the changing relationship of the primary field is linear, the induced current in the steel mesh is a constant value. The induced current distribution in the steel mesh under two conditions is shown on the left side of Figures 2 and 3. According to the principle of linear superposition of current, different current elements can be converted based on the magnitude and direction of the current in the steel mesh.

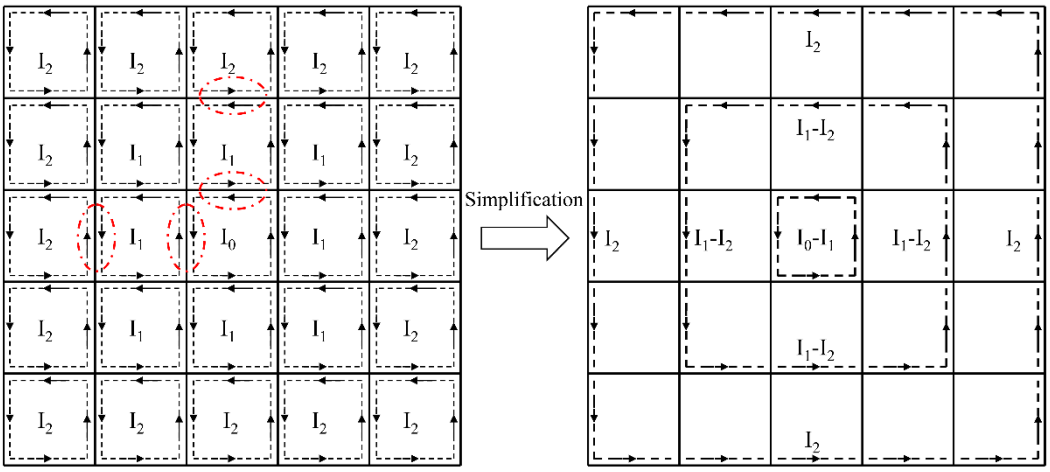

Figure 2. Simplified diagram of the internal current under a uniform magnetic field.

Since the induced current directions of two adjacent grids of the steel mesh are opposite to each other, the induced current generated by the uniform and nonuniform magnetic fields can be simplified. The simplified induced current distribution is shown in Figures 2 and 3. As a result, the induced currents in two circumferential directions and eight ray directions can be simplified in a steel mesh with five intervals. When the magnetic field is a uniform magnetic field, the induced current units in two circumferential directions and eight ray directions are equal and opposite, and the induced current in two circumferential directions and eight ray directions can offset each other, so only the outermost current loop exists. When the magnetic field is a nonuniform magnetic field, the magnitudes of the two circumferential current units are not equal, the directions are opposite, and the two circumferential currents can differ from each other. The eight ray direction current units are equal, the directions are opposite, and the eight ray direction current units can cancel each other, so only three circumferential current loops exist.

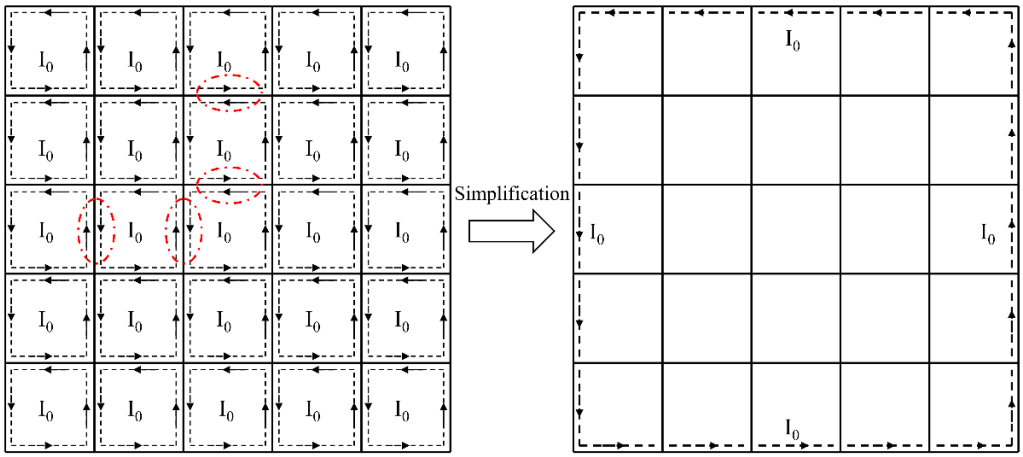

Figure 3. Simplified diagram of an internal current under a nonuniform magnetic field.

When the receiver coil is located in the center of the steel mesh, the induced current generated in the steel mesh generates a secondary field again in the center of the receiver coil. Combined with Eqs (4) and (5), the secondary field of the receiver coil under a uniform magnetic field and nonuniform magnetic field can be calculated. To simplify the form of the magnetic field formula in the receiver coil, the diameter of the steel mesh is not considered for the time being, so the expression for the special case can be obtained as Eqs (6) and (7).

$$B_s = \frac{2\sqrt{2}\mu_0 I_0}{\pi(a+a+0.5a)} = \frac{4\sqrt{2}\mu_0 I_0}{5\pi a} \tag{6}$$

$$\begin{aligned} B_s &= \frac{2\sqrt{2}\mu_0(I_0-I_1)}{\pi a} + \frac{2\sqrt{2}\mu_0(I_1-I_2)}{\pi(a+0.5a)} + \frac{2\sqrt{2}\mu_0 I_2}{\pi(a+a+0.5a)} \\ &= \frac{2\sqrt{2}\mu_0(I_0-I_1)}{\pi a} + \frac{4\sqrt{2}\mu_0(I_1-I_2)}{3\pi a} + \frac{4\sqrt{2}\mu_0 I_2}{5\pi a} \\ &= \frac{2\sqrt{2}\mu_0(15I_0-5I_1-4I_2)}{15\pi a} \end{aligned} \tag{7}$$

where B_s is the secondary field in the receiver coil (Wb/m^2); I_0, I_1 and I_2 are the induced currents of different layers (A), respectively; and a is the spacing of individual steel mesh (m).

Obviously, if I_0, I_1 and I_2 are equal, then Eq (7) can be simplified to Eq (6). Thus, the secondary field formed by the uniform magnetic field can be regarded as a special case of the secondary field formed by the nonuniform magnetic field.

For the convenience of future research, when the interval of the steel mesh is greater than 5, the expression of the secondary field formed by the nonuniform magnetic field is given as Eq (8).

$$B_s = \frac{2\sqrt{2}\mu_0\left(I_0 - I_1\right)}{\pi a} + \sum_{i=2}^{n-1} \frac{4\sqrt{2}\mu_0\left(I_{i-2} - I_{i-1}\right)}{\left(2n-1\right)\pi a} + \frac{4\sqrt{2}\mu_0 I_{n-1}}{\left(2n-1\right)\pi a} \tag{8}$$

where I_0, I_1, I_{i-2}, I_{i-1} and I_{n-1} are the induced currents of different layers (A); n is the total layer number of the current loop ($n \geq 4$); i is the layer number of the current loop; and $2n-1$ is the spacing number of the steel mesh.

For vehicle-mounted transient electromagnetic detection technology, the primary field distribution in the tunnel surrounding rock space is unevenly distributed, so the rectangular steel mesh can be simplified as a multilayer current loop mode. Consequently, a multilayer current loop is formed by the conductor at the multilayer steel mesh, and the conductor of the steel mesh between the layers does not significantly participate in the flow of the induced current. Hence, the secondary field in the receiver coil completely depends on the induced current of the multilayer steel mesh. Combined with the similarity between the rectangular loop and the circular loop, the rectangular loop can be totally simplified to the circular loop in the numerical simulation. Thus, the complex three-dimensional simulation process of steel mesh can be simplified to a simple two-dimensional symmetry model.

2.3. Calculation of a typical fixed interference source

Based on the simplification of the above model, the fixed interference source of the steel mesh in the tunnel structure is still taken as an example, and the calculation and analysis of the numerical simulation model of the fixed interference source can be carried out. According to field and data investigations, four factors of fixed interference sources were selected as numerical simulation objects, namely, distribution length *L*, distribution interval *N*, distance *H* and diameter *D*, as shown in Figure 4. COMSOL MULTIPHYSICS (Version 5.4, COMSOL Incorporation), designed to investigate multifield coupling problems, is chosen as the simulation software. In the software, the AC/DC module is used to solve the electromagnetic field coupling problem according to Maxwell's equations. In the numerical simulation, the resistivity of the fixed interference source is $1.0 \times 10^{-7}\,\Omega\cdot$m, the relative permeability is 1, and the relative dielectric constant is 1. The other parameters of the fixed interference source model are consistent with the numerical simulation model of uniform full-space surrounding rock [4]. Meanwhile, the distance between the fixed interference source and the transmitter coil is set as 6 m because of the constant distance between the water-bearing body and the transmitter coil. The radius and thickness of the water-bearing body are 4 m and 0.3 m, respectively. The detailed finite element model of the surrounding rock, water-bearing body and interference source are shown in Figure 5.

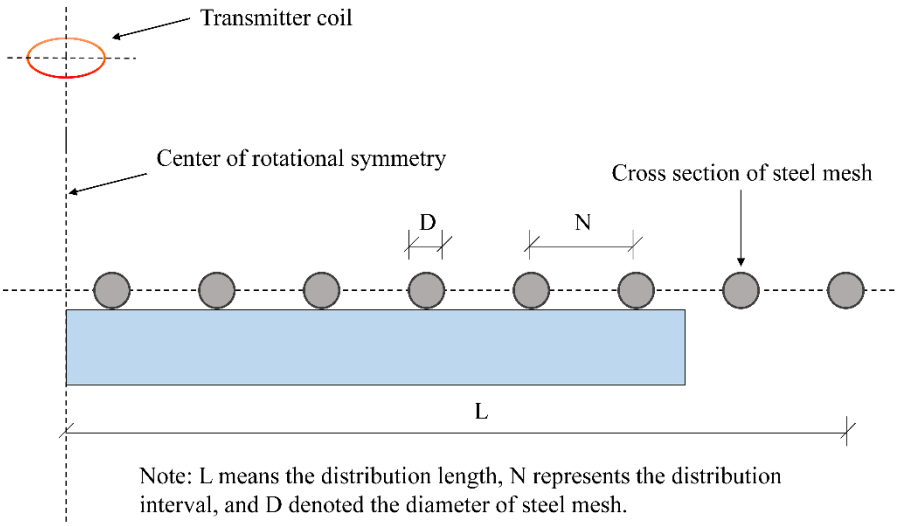

Figure 4. Schematic diagram of simplified model.

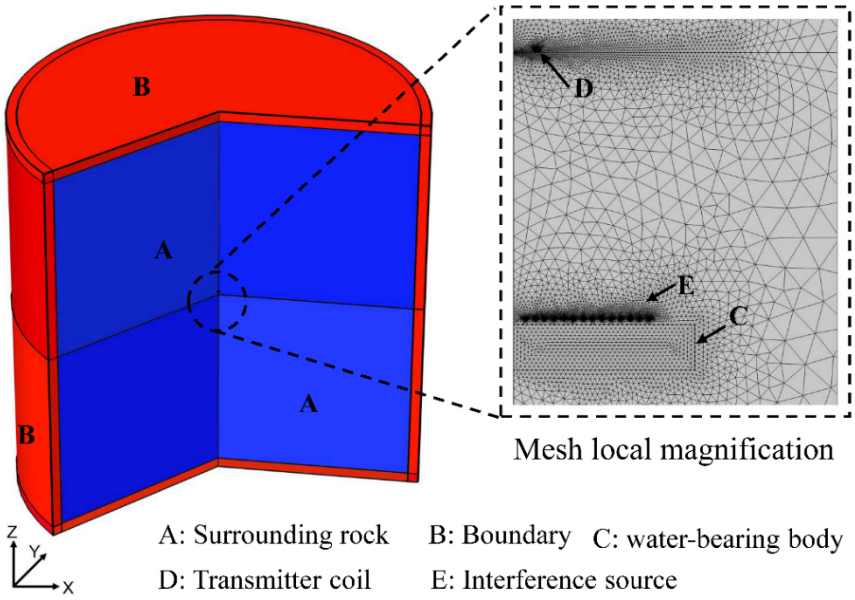

Figure 5. Finite element model of space media.

A typical interference source model is selected as the analysis object, and the transient electromagnetic response of the fixed interference source is calculated. The research parameters of distribution length, distribution interval, distance and diameter are 3 m, 210 mm, 12 mm and 6 m, respectively. Meanwhile, the transient electromagnetic response of uniform full-space surrounding rock was selected as the comparison object [4]. The results are shown in Figure 6.

Based on the simulation results of the two models, the induced voltage response curves of the two models are obviously different. In general, the induced voltage response curve of the fixed interference source is consistent with the induced voltage response curve of uniform full-space surrounding rock in the early stage. The induced voltage response curve of the fixed interference source also presents a linear decrease in the early stage. However, the induced voltage response curve of the fixed

interference source is inconsistent with that of the uniform medium in the middle and late stages. The induced voltage response curve of the fixed interference source shows an obvious lifting phenomenon in the middle stage. The induced voltage response curve slowly decays and presents an approximate horizontal change rule in the late stage.

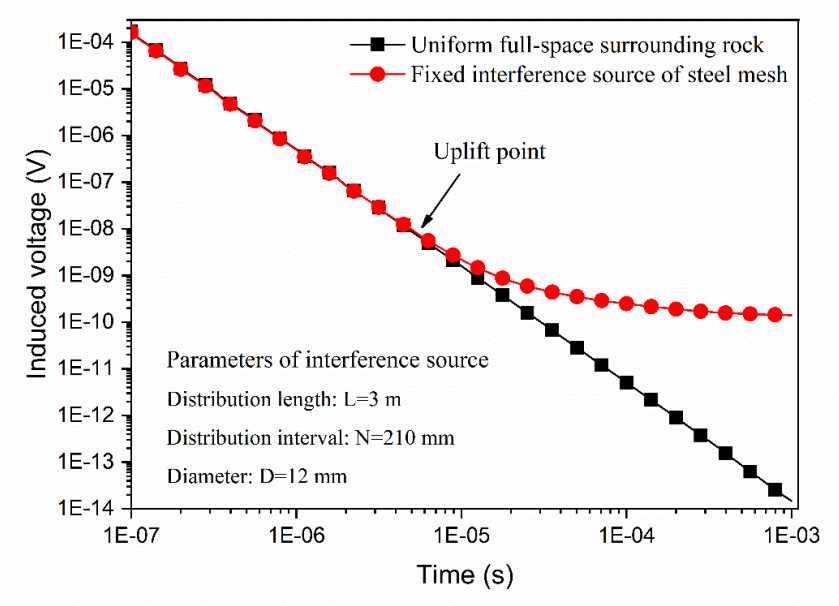

Figure 6. Transient electromagnetic response curve of a fixed interference source model and uniform full-space surrounding rock model.

Meanwhile, compared with the uplift and regression phenomena of the transient electromagnetic response curve in the water-bearing body model [4], the induced voltage response curve of the fixed interference source has no regression phenomenon in the concerned time window. In addition, the corresponding induction time of the induced voltage response curve of the fixed interference source at the uplift point is approximately 10 μs. This value occurs later than the induction time of the water-bearing body, which provides feasibility and possibility for the subsequent superposition of multiple field source signals. From the diffusion mechanism of the induced current, the induced current is concentrated in the surrounding rock in the early stage and shows linear attenuation with increasing induction time. The induced current is transferred to the position of the fixed interference source with the diffusion of the early induced current, and the induced current is concentrated at the position of the interference source in the middle and late stages. Moreover, the induced current attenuates very slowly and does not significantly diffuse outward due to the high conductivity of the fixed interference source.

3. Sensitivity analysis of physical parameters of fixed interference source

According to the previous section, the apparent response characterisation of the fixed interference source mainly depend on the physical parameters of the fixed interference source when the parameters of the surrounding rock remain unchanged. Equations (6)–(8) ignore the influence of the diameter of the steel mesh to quickly reflect the spatial distribution of the magnetic field generated by the current element. In fact, the distribution of the diameter of the steel mesh has a certain influence on the spatial distribution of the magnetic field. Thus, physical parameters that affect transient electromagnetic

signals are chosen in terms of distribution length, distribution interval and diameter. However, the distance between the transmitter coil and fixed interference source remains the same because of the fixed characteristic of the interference source. Meanwhile, the transient electromagnetic signal response characterisation of the fixed interference source are roundly analyzed at different parameter levels. The parameter values of the fixed interference source in the numerical simulation are listed in Table 1.

Table 1. Parameter values of the fixed interference source in the numerical simulation.

Research object	Distribution length (m)	Distribution interval (mm)	Diameter (mm)
Distribution length (*L*)	1, 2, 3, 4, 5	210	12
Distribution interval (*N*)	3	150, 180, 210, 240, 270	12
Diameter (*D*)	3	210	8, 10, 12, 16, 20

3.1. Influence analysis of distribution length

Using the constant of distribution interval and diameter, the influence analysis of the distribution length at different parameter levels can be investigated, and the detailed parameters of the distribution length are listed in Table 1. The transient electromagnetic response curve of the fixed interference source at different distribution lengths is illustrated in Figure 7.

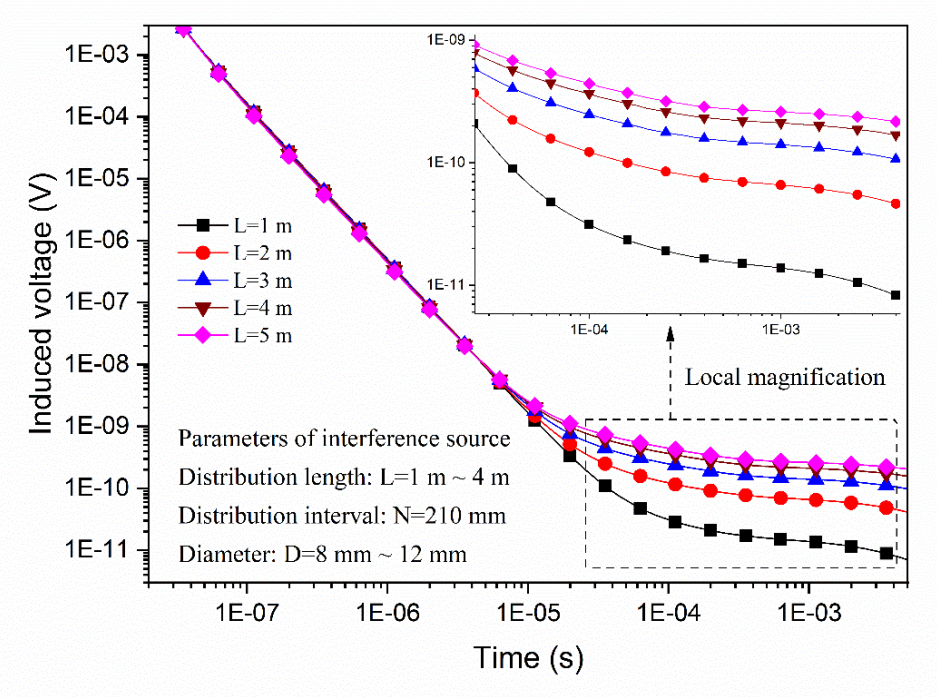

Figure 7. Transient electromagnetic response curve of a fixed interference source at different distribution lengths.

As illustrated in Figure 7, the induced voltage response curve of the fixed interference source has an obvious variation law at different distribution lengths. In the middle and later stages of the response curve, the attenuation of the induced voltage response curve of the fixed interference source is slower,

and the response amplitude is larger when the distribution length is longer. This shows the opposite trend when the distribution length is shorter. By a comprehensive comparison of different distribution lengths, the amplitude of the induced voltage response curve of the fixed interference source increases slowly with a linear increase of distribution length, so the transient electromagnetic response of the fixed interference source is greatly affected by the distribution length. Furthermore, the diffusion radius of the transient electromagnetic "smoke ring" effect limits the influence of the distribution length on the transient electromagnetic response.

3.2. Influence Analysis of distribution interval

The influence analysis of the distribution interval at different parameter levels can be analyzed when the other two parameters are constant, and the detailed parameters of the distribution interval are listed in Table 1. The transient electromagnetic response curve of the fixed interference source at different distribution intervals is presented in Figure 8.

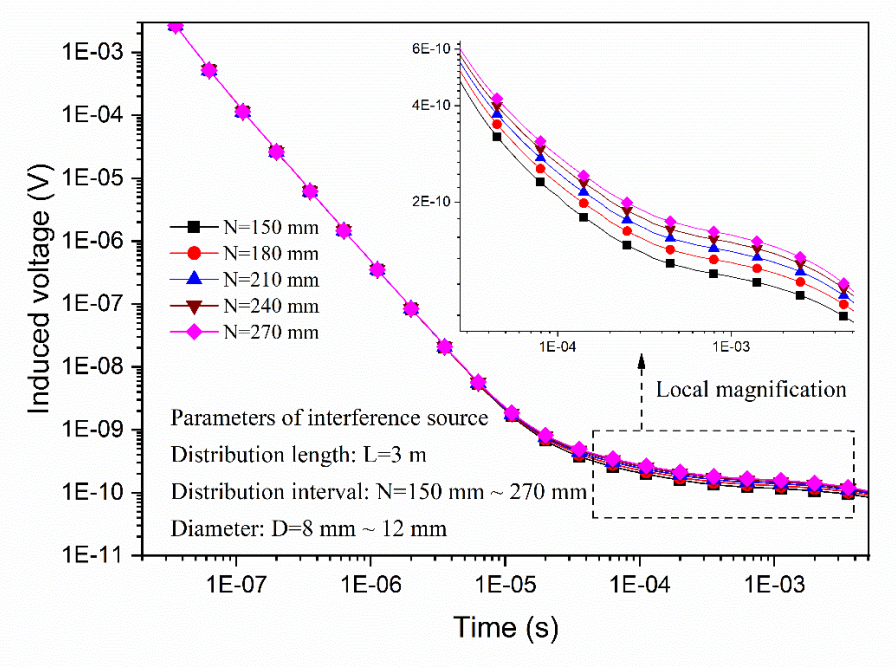

Figure 8. Transient electromagnetic response curve of a fixed interference source at different distribution intervals.

As presented in Figure 8, the induced voltage response curve of the fixed interference source has a weak variation law at different distribution intervals. In the middle and later stages of the response curve, the attenuation of the induced voltage response curve of the fixed interference source is slower, and the response amplitude is larger when the distribution interval is longer. However, the overall trend of this change is not very apparent. As a whole, the amplitude of the induced voltage response curve of the fixed interference source increases very slowly with a linear increase in the distribution interval. This indicates that the transient electromagnetic response of the fixed interference source is not significantly affected by the distribution interval.

3.3. Influence Analysis of diameter

The influence analysis of the diameter at different parameter levels can be researched when the parameters of the distribution length and distribution interval are unchanged. The detailed parameters of the diameter are listed in Table 1. The transient electromagnetic response curve of the fixed interference source at different diameters is depicted in Figure 9.

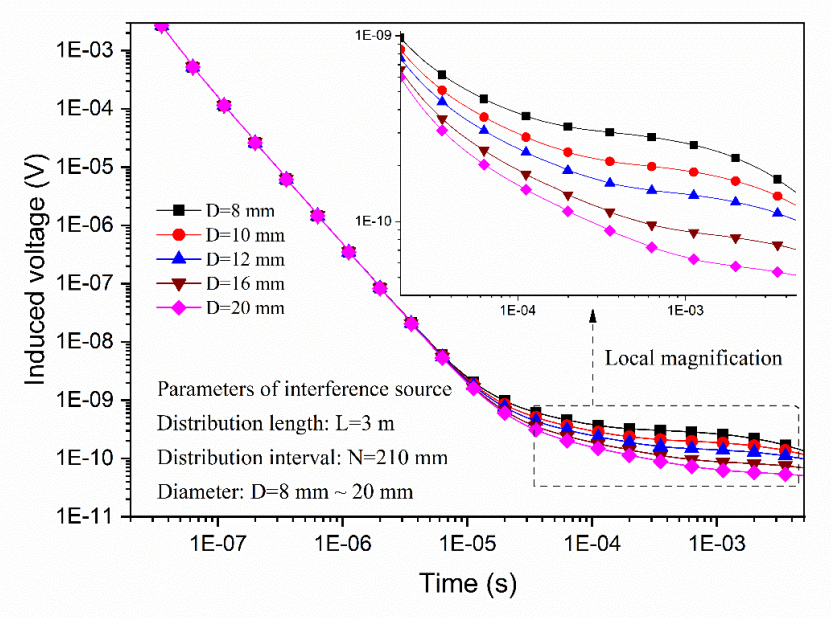

Figure 9. Transient electromagnetic response curve of a fixed interference source at different diameters.

As depicted in Figure 9, the induced voltage response curve of the fixed interference source has a certain variation law at different diameters. In the middle and later stages of the response curve, the attenuation of the induced voltage response curve of the fixed interference source is slower, and the response amplitude is smaller when the diameter is longer. Comparing different diameters of the fixed interference source, the amplitude of the induced voltage response curve of the fixed interference source decreases linearly with a linear increase in the diameter, but the decrease amplitude is limited. Therefore, the diameter has a certain influence on the transient electromagnetic response of the fixed interference source.

Based on the above sensitivity analysis of physical parameters, the distribution length has the greatest influence on the transient electromagnetic response of the fixed interference source, followed by the diameter. The distribution interval has the least influence on the transient electromagnetic response of the fixed interference source.

4. Mathematical superposition method for multiple field sources

4.1. Proposal of mathematical superposition method

Although there are many kinds of interference sources in a tunnel space, the electromagnetic

induction signal of the fixed interference source has a fixed characteristic. Consequently, the transient electromagnetic response generated by these fixed interference sources does not change with the position of the vehicle-mounted detection system. Furthermore, the electromagnetic induction signal generated by multiple field sources is a symbiosis, and the electromagnetic signals of ineffective and effective sources appear, weaken and disappear simultaneously. In three-dimensional space, the characteristic functions of the induced electromotive force of the surrounding rock and water-bearing body are assumed to be $F_s(\rho_s,t)$ and $F_w(\rho_w,t)$, respectively. In addition, the characteristic functions of the induced electromotive force of the first and second types of interference sources are assumed to be $F_1(\rho_1,t)$ and $F_2(\rho_2,t)$, respectively.

For electromagnetic exploration based on the principle of a transient electromagnetic field, the low-frequency electromagnetic field is the main part of the transient electromagnetic field, and the influence of the displacement current can be ignored in Maxwell's equations [5,8,18,19]. Meanwhile, the coupling relationship between multiple sources is not considered, so multiple sources are independent of each other. Thus, the transient electromagnetic induction current generated by different field sources can be linearly superimposed under the condition of a low-frequency electromagnetic field and independent features [8,19]. In the actual operation of the vehicle-mounted transient electromagnetic detection system, the induced electromotive force received by the receiver coil is $e(\rho_s,\rho_w,\rho_1,\rho_2,t)$, and its expression is shown as Eq (9).

$$e(\rho_s,\rho_w,\rho_1,\rho_2,t)=F_s(\rho_s,t)+F_w(\rho_w,t)+F_1(\rho_1,t)+F_2(\rho_2,t) \tag{9}$$

where $e(\rho_s,\rho_w,\rho_1,\rho_2,t)$ is the measured induced electromotive force (V), $F_s(\rho_s,t)$ is the induced electromotive force of the surrounding rock, $F_w(\rho_w,t)$ is the induced electromotive force of the water-bearing body, $F_1(\rho_1,t)$ is the induced electromotive force of the first type of interference source, $F_2(\rho_2,t)$ is the induced electromotive force of the second type of interference source and ρ_s, ρ_w, ρ_1 and ρ_2 are the functions of the spatial distribution and numerical value of the resistivity of the four media, respectively.

The functions $F_1(\rho_1,t)$ and $F_2(\rho_2,t)$ are fixed expressions when the spatial distribution of interference sources is determined. The function of $F_s(\rho_s,t)$ can be calibrated according to the standard tunnel surrounding rock without any water-bearing body. Based on Eq (9), the induced electromotive force of the water-bearing body can be obtained as Eq (10).

$$F_w(\rho_w,t)=e(\rho_s,\rho_w,\rho_1,\rho_2,t)-\left[F_s(\rho_s,t)+F_1(\rho_1,t)+F_2(\rho_2,t)\right] \tag{10}$$

Equation (5) reflects the measured mathematical expression of the electromagnetic induction signal of the water-bearing body, which is an effective electromagnetic induction signal without an interference signal. Furthermore, the spatial distribution characterisation of the water-bearing body can be described according to Eq (5). Therefore, the mathematical separation of effective electromagnetic signals can be preliminarily solved in the process of determining the functional form of the interference source in the electromagnetic environment background field based on the proposed mathematical superposition function.

4.2. Verification based on numerical simulation

Based on the numerical simulation of the fixed interference source model, the water-bearing body behind the fixed interference source is activated and enabled, as shown in Figure 4. The transient electromagnetic response curve both with the interference source and the water-bearing body is calculated as shown in Figure 10. The transient electromagnetic response curves of the homogeneous medium and water-bearing body are also illustrated in Figure 10. In addition, the transient electromagnetic response curve of multiple field sources is obtained by the theoretical mathematical superposition method, and the result is also presented in Figure 10. To compare the calculation results between the theoretical superposition method and the numerical simulation method, the relative error between two calculation conditions is also obtained, as shown in Figure 11.

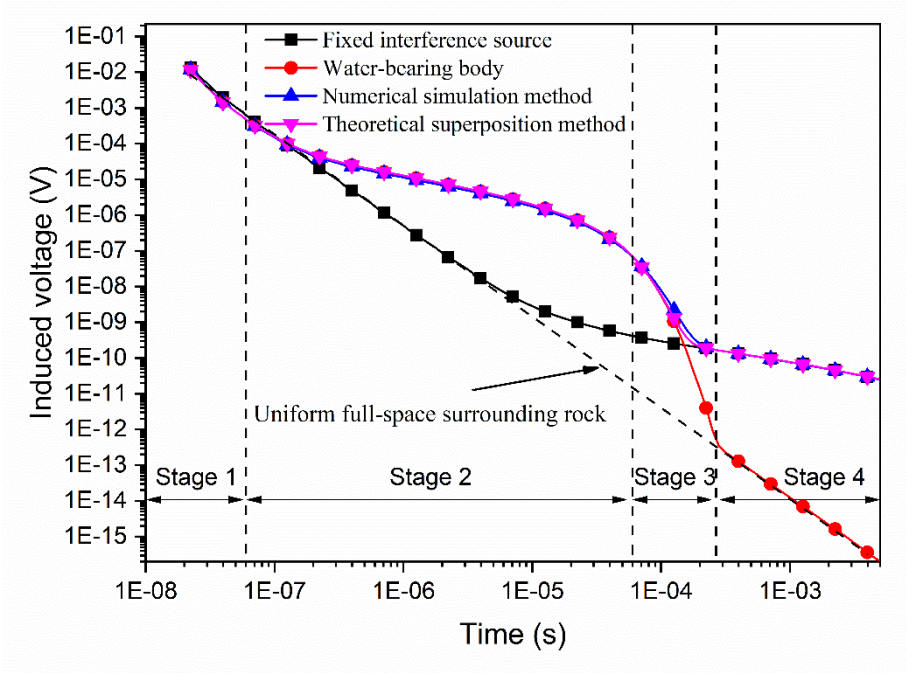

Figure 10. Transient electromagnetic response curves under different media conditions.

As described in Figure 10, the transient electromagnetic response curve of multiple field sources is an independent superposition process between the transient electromagnetic response curve of the water-bearing body and the interference source. In the early and middle stages, the transient electromagnetic response curve of multiple field sources is dominated by the response curve of the water-bearing body. However, the transient electromagnetic response curve of multiple field sources in the late stage is dominated by the response curve of the interference source. Therefore, the transient electromagnetic response curve of multiple field sources illustrates the transient electromagnetic response of different field sources at different time periods. This provides feasibility for separating the transient electromagnetic responses of different field sources. Therefore, the transient electromagnetic response curve obtained by the theoretical superposition method is basically consistent with the transient electromagnetic response curve calculated by the numerical simulation method.

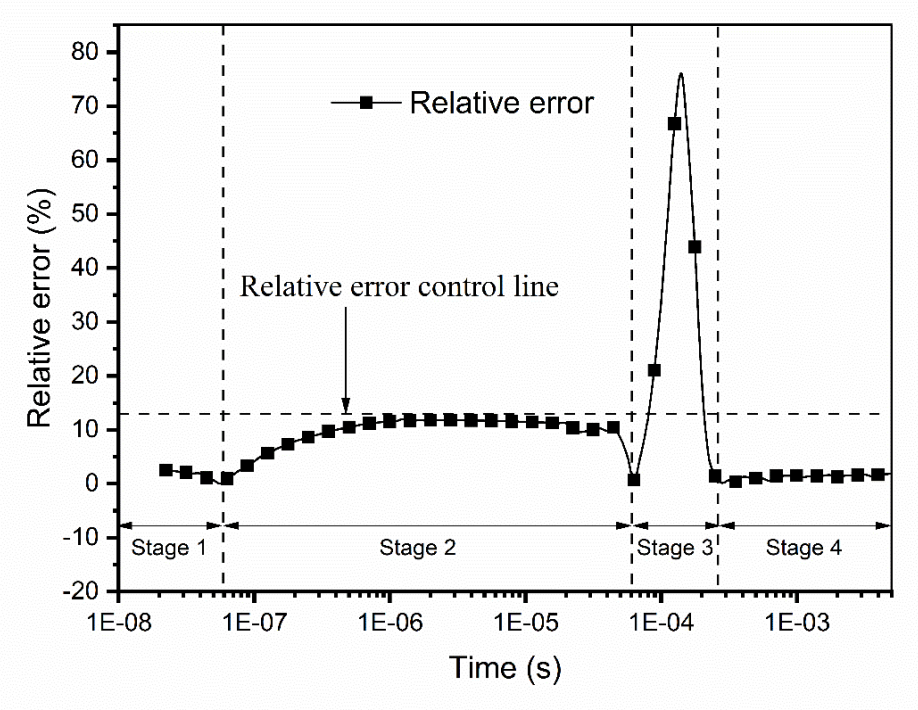

Figure 11. Relative error curve between the theoretical superposition method and the numerical simulation method.

As demonstrated in Figure 11, the relative error curve can be divided into four stages based on the change rule of relative error value between the theoretical superposition method and the numerical simulation method. Similarly, the response curves of multiple field sources calculated by two calculation conditions can also be divided into four stages according to the different stages of Figure 11, as shown in Figure 10. Combining Figures 10 and 11, the curve phenomenon of multiple field sources at different stages can be described together. In the first stage, the response curve of the theoretical superposition method is basically close to that of the numerical simulation method, the result of the theoretical superposition method is lower than that of the numerical simulation method, and the relative error is less than 2.51%. In the second stage, the response curve value of the theoretical superposition method is greater than that of the numerical simulation method, and the maximum relative error is no greater than 11.98%. Meanwhile, the relative error curve of the second stage is maintained for a long time compared with that of the other stages and illustrates a phenomenon of increase, stability and decrease with increasing induction time. In the third stage, the response curves between the two calculation methods are separated first and then closed, and the result of the theoretical superposition method is smaller than that of the numerical simulation method. In addition, the relative error curve presents a phenomenon of rapid increase and decrease, and the maximum relative error can reach 76%. Thus, there is a complex relationship between the water-bearing body and the interference source in the third stage. In the fourth stage, the response curve of the theoretical superposition method almost coincides with that of the numerical simulation method, the relative error curve basically maintains a dynamic change, and the maximum relative error is no higher than 2.92%.

Taking 12% as the relative error control line, it is generally shown that the relative error between two calculation methods is less than 12% in addition to the partial results in the third stage. Convincingly, the results of different calculation methods for multiple field sources are basically

consistent. Therefore, the mathematical separation of transient electromagnetic responses from different field sources can be verified.

5. Discussion

The response characterisation of the transient electromagnetic signal of the fixed interference sources is different from these published literatures, such as Qian et al. [4], Sun et al. [8], and Tamburrino et al. [12]. Furthermore, the difference is mainly reflected in the latter part of the response time, and this is also a unique feature of transient electromagnetic signals of fixed interference sources. Meanwhile, the feature extraction cannot be simply processed compared to the normal situation. The main reason is that the resistivity of the fixed interference source is very different from that of the normal surrounding rock. Besides, the transient electromagnetic signals generated by different media are not a simple linear superposition in the response process, and there is a certain mutual influence between different signals.

For the numerical simulation of the fixed interference source, some simplifications are applied appropriately. There are some gaps between this simplification and the actual situation [14,17], and three-dimensional numerical simulation is urgently needed in the upcoming research. The influence of fixed interference sources in the process of tunnel construction has been verified by the means of field measurement [7,8,19]. For fixed interference sources in operational tunnels, the influence of interference sources in TEM detection also needs further verification.

6. Conclusions

In this paper, the transient electromagnetic characterisation of a fixed interference source in a tunnel structure were investigated, and the mathematical superposition method of multiple field sources was proposed and verified. The main results are as follows: 1) In view of the interference source of the steel mesh, the staggered current distribution can be simplified as a layered current loop, so the complex steel mesh in the three-dimensional model can be simplified to an ordinary steel mesh in the two-dimensional symmetric model. 2) There are obvious differences between the transient electromagnetic response of the interference source and uniform full-space surrounding rock in the middle and late stages. 3) Different physical parameters of the interference source have different sensitivities to the transient electromagnetic response curve of the interference source based on a sensitivity analysis. The sensitivity rank of the physics parameters of the interference source involves the distribution length, diameter and distribution interval. 4) The transient electromagnetic response curves of total field sources demonstrated the response characterisation of different field sources at different time stages. The rationality of separating the different response signals from different field sources was verified.

Data availability

The data used to support the findings of this research are available from the corresponding author upon request.

Acknowledgments

This work was supported by the National Natural Science Foundation of China (Grant Nos. 51808298 and 42007247), Natural Sciences Fund for Colleges and Universities in Jiangsu Province (Grant No. 20KJD560002), Nantong Science and Technology Plan Project (Grant Nos. JC2019107 and JC2020124), Jiangsu Construction System Science and Technology Project (Grant Nos. 2019ZD013 and 2019ZD017), and Jiangsu Province College Students' innovation and entrepreneurship training program (Grant No. 202110304115Y). The authors appreciatively acknowledge the financial support of the abovementioned agencies.

Conflicts of interest

The authors declare that there are no conflicts of interest.

References

1. S. Tian, W. Wang, J. Gong, Development and prospect of railway tunnels in China (including statistics of railway tunnels in China by the end of 2020), *Tunn. Constr.*, **41** (2021), 308–325.
2. F. Ye, N. Qin, X. Liang, A. Ouyang, Z. Qin, E. Su, Analyses of the defects in highway tunnels in china, *Tunn. Undergr. Sp. Tech.*, **107** (2021), 103658.
3. M. Hu, Y. Liu, V. Sugumaran, B. Liu, J. Du, Automated structural defects diagnosis in underground transportation tunnels using semantic technologies, *Automat. Constr.*, **107** (2019), 102929–102929.
4. W. Qian, T. Qi, X. Liang, S. Qin, Z. Li, Y. Li, Vehicle-borne transient electromagnetic numerical characteristic parameter of water-bearing body behind tunnel linings, *Math. Probl. Eng.*, **26** (2020), 8514913.
5. Z. Li, T. Qi, S. Qin, W. Qian, The research on minimizing the induction between the transmitting and receiving coils in close range transient electromagnetic inspection of groundwater-related defects in the operating tunnels, *Math. Biosci. Eng.*, **18** (2021), 4508–4527.
6. X. Liang, T. Qi, Z. Jin, W. Qian, Hybrid support vector machine optimization model for inversion of tunnel transient electromagnetic method, *Math. Biosci. Eng.*, **17** (2020), 3998–4017.
7. Z. Liu, W. Huang, J. Huang, H. Wu, Y. Wang, D. Zhou, Interference of metal materials in tunnels on the detection results by transient electromagnetic method, *Mod. Tunn. Tech.*, **53** (2016), 116–122.
8. H. Sun, X. Li, X. Lu, S. Li, B. Ren, Transient electromagnetic responses in tunnels with strong interferences and the correcting method, A TBM example, *Chin. J. Geophys.*, **59** (2016), 4720–4732.
9. N. Zhou, K. Lei, G. Xue, W. Chen, Induced polarization effect on grounded-wire transient electromagnetic data from transverse electric and magnetic fields, *Geophysics*, **85** (2020), E111–E120.
10. X. Wu, G. Xue, Y. He, J. Xue, Removal of multisource noise in airborne electromagnetic data based on deep learning, *Geophysics*, **85** (2020), B207–B222.
11. B. Blanco-Arrué, P. Yogeshwar, B. Tezkan, D. Díaz, Loop source transient electromagnetics in an urban noise environment: A case study in Santiago de Chile, *Geophysics*, **86** (2021), B135–B147.
12. A. Tamburrino, R. Fresa, S. S. Udpa, Y. Tian, Three-dimensional defect localization from time-of-flight/eddy current testing data, *IEEE T. Magn.*, **40** (2004), 1148–1151.

13. A. Sophina, G. Tian, M. Fan, Pulsed eddy current non-destructive testing and evaluation: A review, *Chin. J. Mech. Eng.*, **30** (2017), 500–514.
14. Y. Li, T. Qi, B. Lei, Z. Li, W. Qian, An iterative inversion method using transient electromagnetic data to predict water-filled caves during the excavation of a tunnel, *Geophysics*, **84** (2019), E89–E103.
15. Z. Guo, G. Xue, J. Liu, X. Wu, Electromagnetic methods for mineral exploration in China: A review, *Ore Geol. Rev.*, **118** (2020), 103357.
16. Q. Di, G. Xue, C. Yin, X. Li, New methods of controlled-source electromagnetic detection in China, *Sci. China Earth Sci.*, **63** (2020), 1268–1277.
17. W. Qian, *Research on Vehicle-mounted Transient Electromagnetic Response Characterisation for Internal Defects of High-speed Railway Tunnel Structure*, Ph.D thesis, Southwest Jiaotong University, 2020.
18. Z. Shi, L. Liu, P. Xiao, Z. Geng, F. Liu, G. Fang, Simulation and analysis of the effect of ungrounded rectangular loop distributed parameters on TEM response, *J. Appl. Geophys.*, **149** (2018), 105–113.
19. J. Zhou, J. Cheng, L. Wen, Response characteristics of metallic facilities and correction method on mine transient electromagnetic surveying, *China Min. Mag.*, **26** (2017), 146–164.

AIMS Press